Font-Pérez, A.; Soriano Martinez, L.; Monzó Balbuena, JM.; Moraes, J.; Borrachero Rosado, MV.; Paya Bernabeu, JJ. (2020). Salt slag recycled by-products in high insulation geopolymer cellular concrete manufacturing. Construction and Building Materials. 231:1-13. https://doi.org/10.1016/j.conbuildmat.2019.117114

Salt slag recycled by-products in high insulation alternative environmentally friendly cellular concrete manufacturing

A. Font[1], L. Soriano[1], J. Monzó[1], J. C. B. Moraes[2], M. V. Borrachero[1] and J. Payá[1*]

[1] GIQUIMA Group - Grupo de Investigación en Química de los Materiales de Construcción. Instituto de Ciencia y Tecnología del Hormigón (ICITECH), Universitat Politècnica de València, Spain.

[2] ITA - Aeronautics Institute of Technology, São Jose dos Campos, São Paulo, Brazil.

* Corresponding author: jjpaya@cst.upv.es; tel: +34 96 387 75 69.

Abstract

This investigation presents an important contribution to the understanding of the "zero discharge in the aluminium cycle" goal. The salt slag recycled by-product was reused as alternative aerating agent in the manufacture of cellular concretes: fluid catalytic cracking catalyst (FCC) – based geopolymer (GCC) and blast furnace (BFS) – based alkali-activated (AACC). The hydrogen emission test was used to evaluate the gas releasing properties because of the presence of metallic aluminium in the salt slag. Density (kg/cm^3), compressive strength (MPa) and thermal conductivity (W/mK) for GCC were 75, 6.9 and 0.31 and for AACC were 602, 7.5 and 0.16.

Keywords: Aluminium salt slag recycled by-product**,** cellular concrete, geopolymer, alkali-activation, thermal insulation, waste valorisation

Abbreviations:
TCC: Traditional cellular concrete
GCC: Geopolymer cellular concrete
AACC: Alkali-activated cellular concrete
OPC: Ordinary Portland cement
FCC: Fluid catalytic cracking residue
BFS: Blast furnace slag
PG: Granulated paval
FCCPGm: FCC and PG co-milled
BFSPGm: BFS and PG co-milled

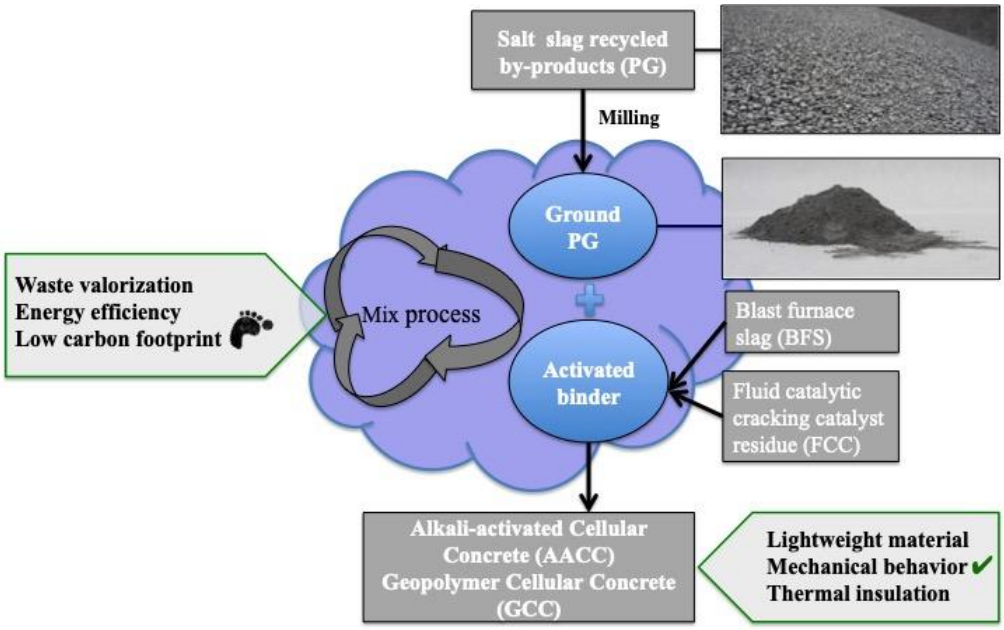

GRAPHYCAL ABSTRACT

1. Introduction

Traditional concrete is the most popular construction material because of its excellent structural and durability properties and consistent availability [1,2]. Many concrete applications require a high-density material (above 1800 kg/m^3); however, in special cases, lower-density materials yield more benefits. In this respect, the cellular concrete is a low-density material that represents an interesting cost-effective alternative material to traditional concrete because of the total material volume savings. This is because the air content is between 10% and 70% [3].

Traditional cellular concrete (TCC) is a cement - based material (with sometimes lime additions) with a structured void-system matrix that results from the addition of a physical or chemical expansion agent. This material is normally manufactured with no aggregates or sand, and a partial replacement of binder can be found by pozzolanic materials to improve its properties[4]. The chemical reagent most commonly used is aluminium powder, which, in contact with the alkaline medium (calcium hydroxide) from the cement, liberates hydrogen gas, as shown in Equation 1[5]. When this chemical reagent is added, a curing treatment in an autoclave (high-pressure steam curing) is usually applied. This curing method reduces the setting time and improves the early-age strength, increases the durability and reduces the drying shrinkage and moisture movement [6]. This material is commonly known by authors as autoclaved aerated concrete (AAC) [5–8], where:

$$2Al + 3Ca(OH)_2 + 6H_2O \Rightarrow 3CaO \cdot Al_2O_3 \cdot 6H_2O + 3\,H_2 \quad (1)$$

Aluminium powder + hydrated lime + water $\Rightarrow$ *tricalcium aluminate hydrate + hydrogen*

Because of the internal void system configuration that characterizes TCC, this material has low-density, moderate mechanical behaviour and good thermal and acoustic performance. It has a self -flowing behaviour in the fresh state and it is easily pumped without compaction requirement to place it [6]. The material is commonly employed to make masonry units, such as bricks, flooring, trench filling and several insulation applications. B. Dolton et al. [4] introduced the TCC as more durable than traditional insulating materials because of its high resistance of chemical and fire exposure. Despite its great advantages, TCC manufacturing involves critical drawbacks when the environment, energy and economic issues are considered.

Traditional cellular concrete is mainly composed by ordinary Portland cement (OPC) [9] which main component is clinker. The manufacturing of clinker involves a substantial energy, the consumption of non-renewable raw materials (e.g. limestone, clay and marl,) and around 8% of the anthropogenic CO_2 emissions in the world [10]. In order to address the phenomenon of global warming and the corresponding

environmental impact, the application of new alkali-activated cements, or geopolymers, in the cellular concrete technology is currently investigated.

The new alkali-activated cements, or geopolymers, are inorganic polymeric materials whose manufacture involves a chemical reaction between amorphous alumino-silicate raw materials with highly concentrated aqueous solution alkali compounds (i.g silicates and hydroxides). The process yields stable three-dimensional polymeric structures. The production of "green concrete" has the following advantages: (i) notice high strength, (ii) lower energy requirement and beneficial environment impact from low CO_2 emissions [11] and (iii) beneficial impact of by-products and wastes by recycling. Diverse types of by-products and wastes are generally reported as suitable precursors for preparing cellular concretes by using geopolymeric binders (fly ash, metakaolin or spent FCC catalyst with low Ca content) as well as alkali - activated materials (blast furnace slag with high Ca content) [12–15].

The autoclave treatment required for TCC involves high temperature and pressure conditions, which raises important energy consumption and economic issues. The new GCC and AACC can be cured at ambient temperatures as well as at temperatures in the range 70ºC – 90ºC and achieve a stable matrix and suitable physical and mechanical behaviour. Recently, Font et al. [14] reported FCC-based GCC cured at room temperature (23ºC/100% RH) with a density of 690 kg/m^3, compressive strength of 3.5 MPa and thermal conductivity of 0.581 W/mK. Aguilar et al. [16] presented cellular concretes with metakaolin and fly ash that yielded 600 kg/m^3, 1.7 MPa and 0.470 W/mK when the GCC was cured at 20ºC. The AACC cured at a high temperature (87ºC) was investigated by H. Esmaily [13], who used blast furnace slag and with the product had a density of 681 kg/m^3 and 1 MPa compressive strength.

The production of 1 kg of primary aluminium from aluminium oxide (alumina, Al_2O_3) requires 15.7 kWh of electricity per the commonly used Hall-Héroult process [17]. To obtain alumina from bauxite, the Bayer process is generally employed. This process consists of grinding, digesting, dissolving, filtering, cooling, precipitating and drying sub-processes that require 13 kWh of electricity and result in 1-2 tons of residues for the production of 1 ton of alumina [18]. Furthermore, the obtained primary aluminium needs to be ground to a powder through stamp milling, ball milling under dry conditions, wet ball milling, attrition milling or vibration milling [19]. The high-energy consumption and residues that are generated from the production of primary aluminium powder have a harmfully environmental impact. Because of the high recyclability of the wasted aluminium products, the secondary aluminium production allows an energy savings of 95%. Currently, the European production of aluminium is near 87% for the secondary production process [20]. In Europe, 4 million tons of recycled aluminium are annually processed from the packaging, construction and transport sectors [21].

The search for an aerating reagent alternative for aluminium powder in the manufacturing of traditional cellular concretes has been carried out by several authors. The replacement of aluminium powders in the cellular concrete manufacturing process by recycled scrap [22], residues from an energy pilot plant (gasification) [8], ashes from municipal solid waste [23] and aluminium foil [14] have been described in recent investigation reports.

Salt slags are the residues generated from the metal fusion in secondary aluminium production, where 1 ton of aluminium leaves 0.5 ton of salt slags, which may have different particle sizes as well as variable contents of aluminium, melting salts and aluminium oxide. The treatment and valorisation is carried out in specialized plants from which it is possible to recover the 5% of metallic aluminium, 45% of melting slags and 50% of the new by-product currently known as Paval [21] (Figure 1). In 2017 the 80000 – 90000 tons annual production of Paval in Befesa Aluminio S.L plant (Valladolid, Spain) has been reported. This means that all of this waste is fully converted into raw materials that can be used by the industry. The Paval by-product that is obtained in the recycling plants is ground and classified in three size fractions: i) 0 – 250 μm, referred to as Paval, Serox or BFA; ii) < 45 μm, referred to as Fine Paval (PF); and iii) 0.7 – 1.5 mm, referred to as granulated paval (PG). Since the first two size fractions are composed of 70% alumina, these provide an appealing alternative to conventional bauxite. These have been successfully used as an alternative aluminium corrector in the manufacture of OPC clinker in a number of countries, including Spain, Germany, the UK and France. However, the thicker fraction, PG, includes some fine fractions of metallic aluminium particles. Thus, their reuse is not feasible because of the reactivity of the metallic aluminium.

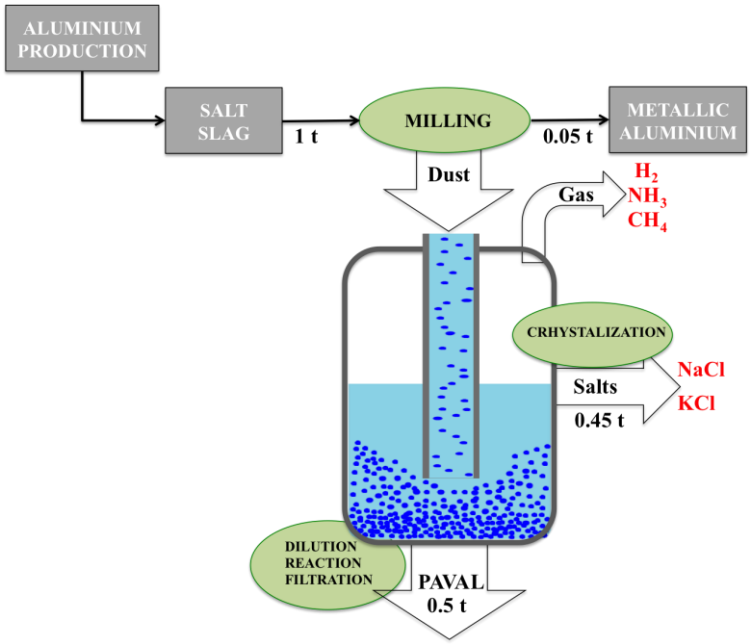

Figure 1 Recycling process diagram of salt slag from secondary aluminium production [21].

This research aims to study the granulated paval (PG), a by-product obtained from the processing of salt slag, as an aerating reagent in new geopolymer cellular concretes (GCC) with fluid catalytic cracking catalyst residue (FCC) and alkali-activated cellular concretes (AACC) with blast furnace slag (BFS) manufacturing. The PG was first mechanically treated and fully characterized and then it was tested as an aeration agent in the GCC matrix. The incorporation of PG in the GCC and AACC pastes was studied and compared with the use of the traditional commercial powered aluminium (A).

2. Materials and methods

2.1 Materials

Two solid precursors were selected to design the GCC and AACC aerated by the PG addition: i) FCC that was supplied by BP Oil Company (Grao de Castellon, Spain) and ii) blast furnace slag (BFS) that was supplied by Cementval S.A (Puerto de Sagunto, Spain). The chemical compositions of the FCC and BFS were analysed by X-Ray fluorescence (XRF) equipment (Magic Pro Spectrometer-Philips) and are shown in Table 1 [14,24]. The X-ray diffractogram patterns of both precursors, FCC and BFS, are shown in Figure 2. For the FCC the main peaks correspond to faujasite ($Na_2Al_2Si_4O_{12}8H_2O$, PDFcard: 391380) and minor peaks of mullite ($Al_6Si_2O_{13}$, PDFcard: 150776), albite ($NaSi_3O_8$, PDFcard: 711152) and quartz (SiO_2, PDFcard: 331161) can also observed. In the case of BFS an amorphous pattern can be observe with some characteristic peaks of quartz (SiO_2, PDFcard: 331161) and calcite ($CaCO_3$, PDFcard: 050586).

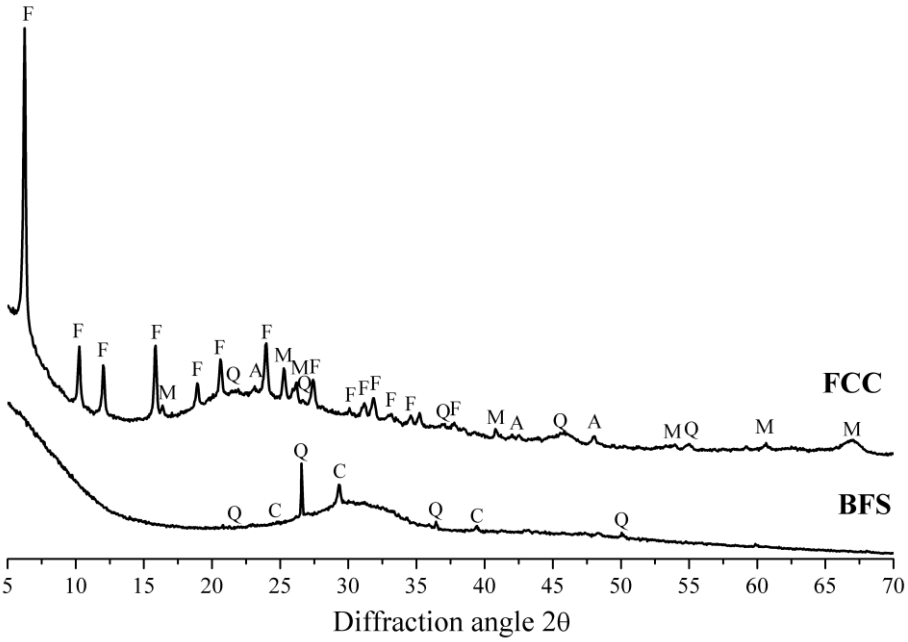

Figure 2 X-ray diffraction pattern of FCC and BFS (Key: F, faujasite; M, mullite; A, albite; Q, quartz; C, calcite).

In order to obtain a finer material and improve their alkali reactivity, 450 g of these solid precursors, previously dry (24 hours at 100 ºC), were milled with 98 alumina balls. The FCC was milled for 20 minutes and had a mean particle diameter (D_{mean}), d_{10}, d_{50} and d_{90} equal to 18.91 µm, 0.21 µm, 11.72 µm and 49.05 µm, respectively. The BFS was milled for 30 minutes and had a D_{mean}, $d_{10,}$ d_{50} and d_{90} equal to 28.80 µm, 2.81 µm, 19.71 µm and 68.89 µm, respectively. The particle size of FCC and BFS was measured by means of a Malvern Instruments Mastersizer 2000 (in water suspension) and the distribution of both materials is shown in Figure 3

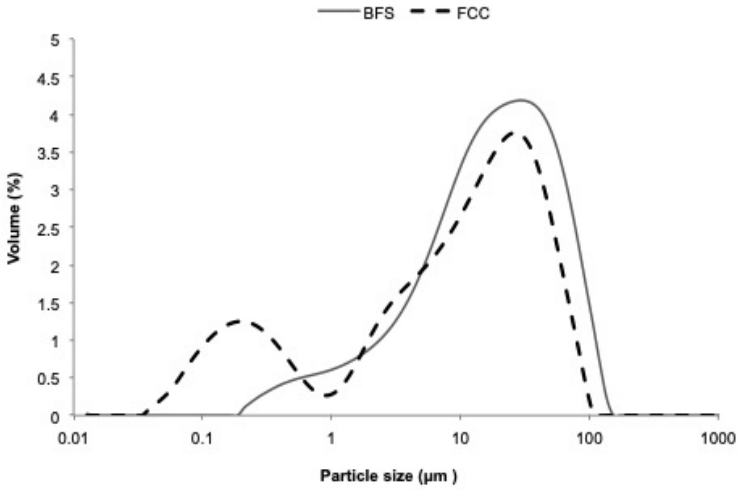

Figure 3 Particle size distribution curves for BFS and FCC.

To prepare the alkaline solutions, water glass (8% Na_2O, 28% SiO_2 and 64% H_2O) and sodium hydroxide pellets (98% purity) were used. Both were acquired from Merck.

Granulated paval (PG) from Befesa Aluminio S.L (Valladolid, Spain) is the alternative reagent used for the GCC aeration in this investigation. The PG is produced by salt slag recycling, which is a waste produced by the secondary aluminium industry. Its chemical composition is also shown in Table. The chemical

composition of PG was extracted from 2016 annual report supplied by Befesa Aluminio S.L. The PG is mostly composed of Al_2O_3 (80.57%). Commercial aluminium powder (A) was used for the control GCC sample aeration. It was supplied by Schlenk Metallic Pigments GmbH and had a 30 µm mean particle diameter.

Table 1 Chemical compositions of FCC, BFS and PG (wt%).

	SiO_2	Al_2O_3	Fe_2O_3	CaO	MgO	SO_3	K_2O	Na_2O	P_2O_5	TiO_2	Others	LOI*
FCC	47.76	49.26	0.60	0.11	0.17	0.02	0.02	0.31	0.01	1.22	-	0.53
BFS	30.53	10.55	1.29	40.15	7.43	1.93	0.57	0.87	0.26	0.89	-	5.53
PG	10.37	80.57	1.04	2.00	0.67	0.44	0.65	1.50	0.13	0.16	1.5	0.97

*Loss on ignition

2.2 Methods

The experimental procedure in the present work is divided in the two sequential steps shown in Figure 4 where the employed methods in each one are indicated.

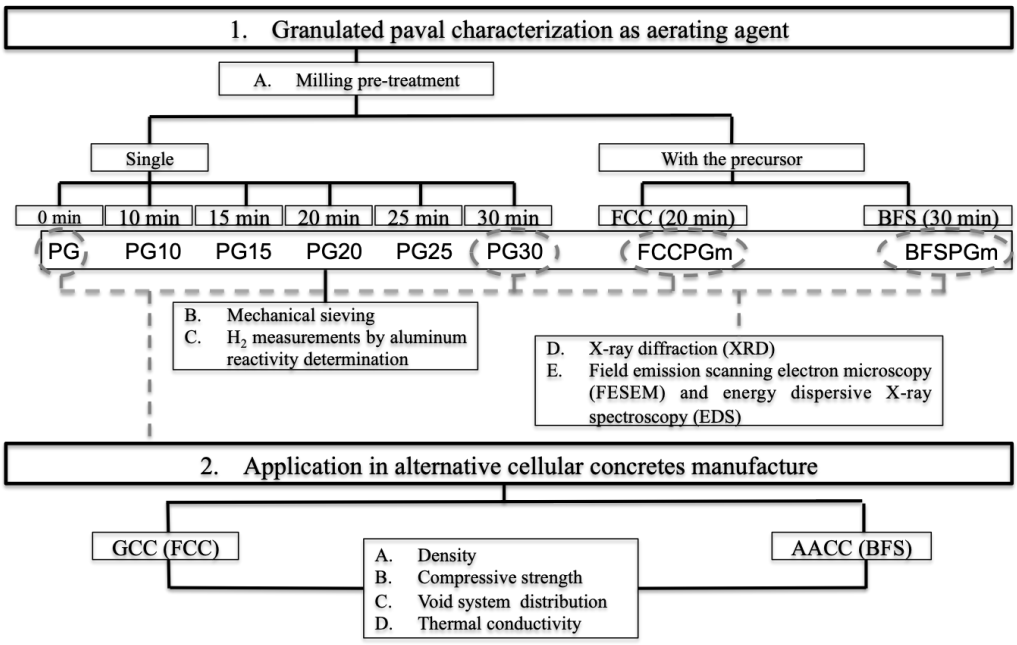

Figure 4 Overview of experimental procedure

2.2.2 Granulated paval characterization

The aerated cellular concrete structure (matrix void system distribution) and its physical properties are directly related with type and size of reagent added [7]. The original PG was milled in a Gabrielli Mill-2 ball mill by two methods. One method was done without precursor for 10, 15, 20, 25 and 30 minutes and whose resultant samples were referred to as PGX, where X represents the milling time in minutes (PG10, PG15, PG20, PG25 or PG30). The milling process was carried out with 250 g of dry material (24 hours at 100 ºC) and 98 alumina balls. The other method included 2% by mass of precursor in the milling procedure. The milling parameters described above ("2.1 Materials" section: 450g of dry material with 98 alumina balls, during: i) 20 minutes when the FCC is the precursor; and ii) 30 minutes when BFS is the precursor) were also used and the resultant samples were referred to as YPGm, where Y represents the corresponding raw material (FCCPGm or BFSPGm).

All of these resultant materials were characterized in terms of particle size distribution by mechanical sieving in dry state. Considering that the PG reaction comes from its aluminium (metal) content, H_2 measurements were carried out by aluminium reactivity determination test used by Font et al. [14]. This

method considers the aluminium oxidation when it comes in contact with high alkali solution (NaOH, 7.5M) and measures the displacement of a water column by the released H_2 (Equation (2)). Five measurements for 0.01, 0.05, 0.08, 0.1, 0.5, 1 and 1.5 g of each tested material were carried out and the equivalent arithmetic mean was calculated. The results that differed by more than 10% were rejected.

$$Al\ (s) + 3H_2O + OH^-_{(ac)} \Rightarrow Al(OH)_4^-_{(ac)} + 3/2\ H_{2\ (g)} \quad (2)$$

Aluminium powder + water + hydroxide ⇒ aluminate + hydrogen

The original PG, the PG milled for 30 minutes (PG30) and the resultant material from the precursor and PG milled together (FCCPGm and BFSPGm) were characterized by X-ray diffraction (XRD) and field emission scanning electron microscopy (FESEM) with energy dispersive X-ray spectroscopy (EDS). Both of tests were carried out to powder samples. The XRD patterns were obtained using a Bruker AXS D8 Advance in the 2θ range of 5º – 70º. The FESEM micrographs were taken by an ULTRA 55-ZEISS with a powder sample covered by carbon, and the EDS test was carried out with a 6-8mm working distance and extra high voltage of 20kV.

2.2.3 Application in alternative cellular concretes manufacture

In Table 2 the experimental procedure to geopolymer cellular concrete preparation and characterization is summarized.

Table 2 Experimental data to geopolymer cellular concrete preparation and characterization.

Sample **(XyZ)**	Precursor **(X)**	Aerating agent		**Water /binder**		**Alkali solution**		**Tests***	
		% **(y)**	Type **(Z)**	64 cm^3	1000 cm^3	SiO_2/Na_2O	Na^+	64 cm^3	1000 cm^3
FCC2PGm	FCC (500g)	2	PGm	0.5	0.6	1.7	7.5	D Rc VSD (7 and 28 days)	D Rc TC (28 days)
FCC1PG30		1	PG30						
FCC1.5PG30		1.5							
FCC2PG30		2							
FCC5PG		5	PG						
FCC10PG		10							
FCC0.2A		0.2	A						
BFS2PGm	BFS (500g)	2	PGm	0.3	0.35				
BFS1PG30		1	PG30						
BFS1.5PG30		1.5							
BFS2PG30		2							
BFS5PG		5	PG						
BFS10PG		10							
BFS0.2A		0.2	A						

* D: Density; Rc: Compressive strength; VSD: Void system distribution; and TC: Thermal conductivity.

The three different states of granulated paval with different percentages of addition were assessed for the GCC samples, with either FCC or BFS, as follows: i) without milling pre-treatment, in the original state (PG), in 5% and 10% proportions by mass with respect to the precursor; ii) with previous 30 minutes milling pre-treatment (PG30), in 1%, 1.5% and 2% proportions by mass with respect to the precursor; and iii) by precursor and PG co-milling (FCCPGm and BFSPGm) in 2% by mass with respect to the precursor. This difference in addition percentages between PG and PG30 was determined from the hydrogen emission tests results, as described in detail in the in Results and Discussion section below.

Depending on the test carried out, two casting moulds were used for each sample: i) nine 4x4x4 cm cubes to measure the density, compressive strength (after 7 and 28 curing days) and void system distribution; and ii) eight 10x10x10 cm cubes to measure density, compressive strength and thermal conductivity after 28 days. For the 64 cm^3 sample production, a normalize mixer machine [25] with 5 litres of capacity was employed. An AEG SBE705RE power drill connected with a paint mixer was used to produce the 1000 cm^3 samples. The differences in the mixed volume and the mixing method had an influence in the material rheology and, consequently, the liquid phase stoichiometry had to be readjusted. For the alkali solution preparation, the SiO_2/Na_2O molar ratio was 1.7 with Na^+ molality of 7.5 and the water/binder (w/b) ratio varied depending on the casting mould used as follows [15]:

i. FCC samples: for 64 cm^3 w/b = 0.5 and for 1000cm^3 w/b = 0.6
ii. BFS samples: for 64cm^3 w/b = 0.3 and for 1000 cm^3 w/b = 0.35.

The samples were cured at room temperature (23ºC and 100% R.H) for 24 hours. At this time, the free surfaces of the cubes were cut with a saw blade and the specimens were de-moulded. Finally, the samples were kept in wet chamber until testing.

The sample designation in this paper is *XyZ*, where *X* the raw material (FCC or BFS), *y* is the percentage of PG incorporated (*y*= 5, 10, 1, 1.5 or 2) and Z is the method of PG addition into the samples (original state = PG, milled during 30 minutes = PG30 or milled with the precursor = PGm). For the control samples, the designation is FCC0.2A and BFS0.2A, which had 0.2% commercial aluminium powder (A) by mass of the precursor.
The natural densities of the alternative cellular concretes were determined immediately after demolding by the specimen weight per unit of volume and the compressive strength was measured in an INSTRON 3282 universal testing machine [26]. The void system was characterized with FESEM micrographs and optical microscopy (OM) photographs. A Leica S8 APO optical microscope was used and the pictures were taken by a Leica DFC 420 digital camera. The images were processed using the Leica LAS image analysis software. The void measurements in the FESEM micrographs and OM images considered an spherical/spheroidal shape for the voids. The thermal conductivity measurements were carried out with a KD2-Pro handheld device (Decagon Devices Inc.) with a complementary thick (6 cm long, 3.9 mm diameter) single RK-1 sensor based on the dual needle probe system (transient line source method) according to ASTM D5334-14 and IEE 442-1981 [27,28]. Before the measurements, a standard (RH-1-01116, 0.387±10% W/mK) was used to verify the good performance of the sensor.

3. Results and discussion

3.1 Granulated paval characterization

Table 3 shows the granulometric parameters that were obtained by sieving the PG samples. The original PG (without milling) had very large particles, with more than 96% greater than 250 µm. The percentage of 250 µm particles was drastically reduced by grinding. In PG10 (10 minutes grinding), it was 38.2% and in PG30 (30 minutes grinding), it was only 18.5% by mass.

Table 3 Particle size distribution (sieved in the dry state) for PG and ground PG samples (from 10 to 30 minutes grinding), FCC and BFS, and for PG milling jointly with catalyst residue (FCCPGm) or blast furnace slag (BFSPGm).

	Particle size distribution				
	>250 µm	250-125 µm	125-63 µm	63-45 µm	<45 µm
PG	96.7	1.0	1.5	0.7	0.0
PG10	38.2	35.2	9.6	12.8	4.1
PG15	32.8	20.5	21.4	14.1	11.1
PG20	29.6	6.8	22.0	26.2	15.4
PG25	23.7	4.6	31.4	7.1	33.2
PG30	18.5	5.4	25.8	16.8	33.5
FCC	0	0.3	1.5	29.6	68.6
FCCPGm	0	0.3	1.1	24.5	74.1
BFS	0	0.3	2.3	44.1	53.3
BFSPGm	0	0.2	2.2	49.7	47.9

The aerating reaction in the alkaline medium increased with the particle fineness. The metal powders commonly added into cellular concretes have an average grain size of 20 - 45 µm [29]. The PG30 contained

over 50% of particles with a grain size less than 63 µm, which was the most similar to the commercial powder among the PG samples. The remaining shorter milling times yielded larger particle sizes. Furthermore, PG30 was significantly coarser than the precursors. Most of particles for FCC and BSF were smaller than 63 µm.

For the samples of PG and precursor that were co-milled (FCCPGm and BFSPGm), it was found (Table 3) that also most of the particles had a size lower than 63 µm. This means that, by this procedure and in view of the results for the PG singly milling treatment (in all of milling experimented times), the PG particles were comminute to a similar particle size as the precursor. One of the most influential parameters on the effectiveness of the matrix aeration in the cellular concretes is the aluminium particle oxidation. The volume of liberated hydrogen into the alkaline medium (NaOH or KOH aqueous solution) is directly related to the aluminium content, initial alkali concentration, temperature and aluminium particle surface area [30]. A larger surface area allows better impregnation of the aluminium particles when they come in contact with the alkali solution. The reaction of the aluminium with the alkali solution starts with the hydration of the Al atoms and the chemisorption of the hydroxide ions [31]. A first-order topochemical redox reaction takes place. The inclusion of the alternative recycled aluminium foil in the milling treatment of the FCC as of the BFS was studied by Font et al. [14,15] with great results. The foil pre-treatment reduced its particle size. The co-milling of the precursor and aluminium did not significantly modify the granulometric distribution of the obtained powder compared to the ground precursor without aluminium foil.

The considered reference dosage of A to the cellular concretes was 0.2% (with respect the weight of precursor), and the entire A was reactive in the alkaline medium. The dependence between the resultant percentages of the equivalent reactive aluminium for each tested material (original PG and samples milled during different times) and the percentages of each material to incorporate 0.2% of aluminium in GCC manufacture are shown in Figure 5.

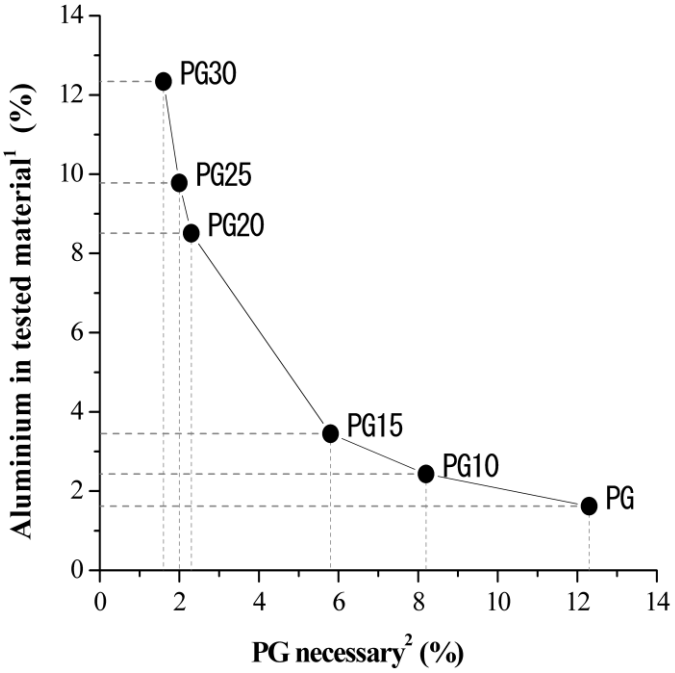

Figure 5 Results of H_2 emission tests.
[1]reactive metallic aluminium content in each tested material; [2] percentage of each PG type to add in the manufacture of GCC and AACC with 0.2% of reactive metallic aluminium.

The PG (0.1g) in its original size liberated 50 mg of H_2, which indicates that the reactive metallic aluminium content was 1.8% by weight (see Y-Axis in 43). Consequently, to incorporate 0.2% (by weight) of reactive aluminium in a GCC or AACC sample, a PG addition between 12% and 13% is necessary (see X-axis in Figure 5). In the other extreme modality proposed, when PG is milled for 30 minutes (PG30

sample), the liberated H_2 from 0.1g increases to 100 mg, which means there was 12.2% of reactive aluminium metallic content. Consequently, the amount of PG30 necessary to incorporate 0.2% (by weight) of reactive aluminium in GCC or AACC sample decreased to 1%-2%. It can be noted that when the milling time increases, the amount of treated PG to yield 0.2% of reactive metallic aluminium addition equivalent in the GCC or AACC samples decreases.

A controlled aerated reaction is essential to develop a good void system structure. This influences the physical behaviour of the cellular concretes. The reaction in a basic medium of the metallic aluminium contained in PG is the basis to carry out the study of its application in GCC as well as AACC mixes. The particle size difference between PG and PG30 involves a high yield of H_2 gas emissions. Consequently, a lower quantity of material must be added to incorporate the equivalence of 0.2% of metallic reactive aluminium into the mixes. The influence of the particle size in the aeration effect has been recently verified by authors that presented commercial aluminium powder alternatives for cellular concrete aeration [14,22,23].

Based on these results, PG and PG30 and the innovative co-milling with the corresponding precursor (FCCPGm and BFSPGm) processes were selected for addition to the designed geopolymer cellular concretes. The percentages (with respect the precursor weight) assessed in the samples were: 10% and 5% in the case of PG addition; 1%, 1.5% and 2% for PG30 addition; and 2% for FCCPGm and BFSPGm.

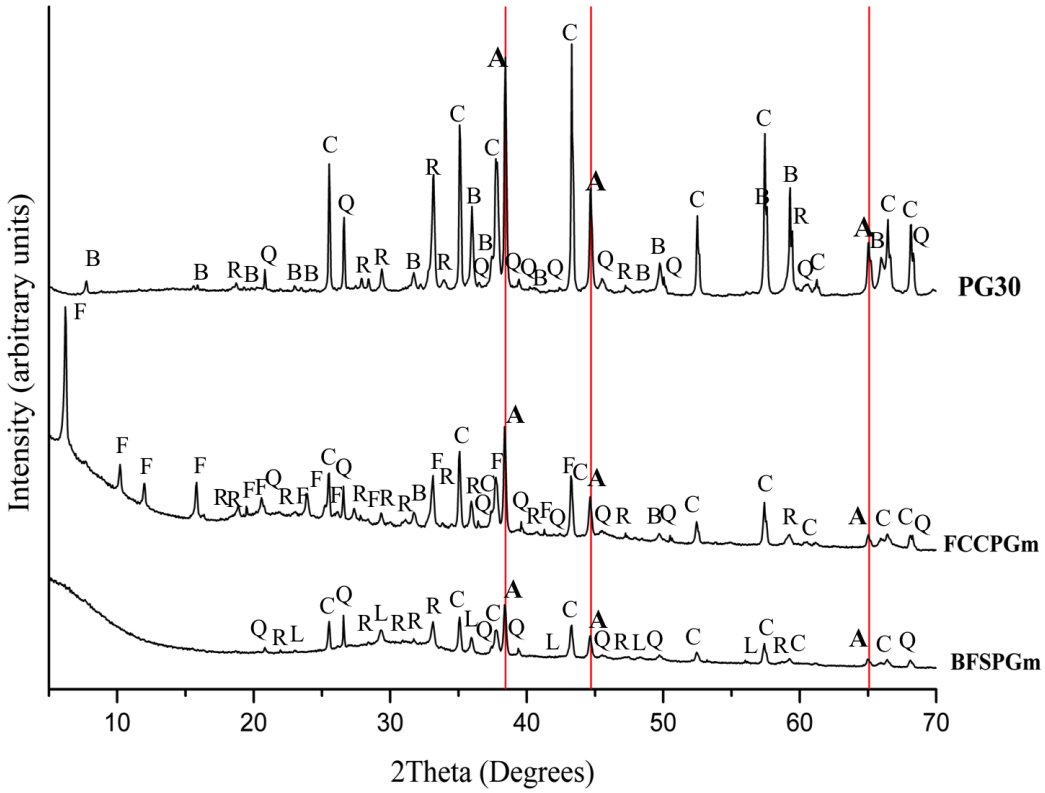

Figure 6 X-ray diffractograms for PG30, FCCPGm and BFSPGm. (Key: Q – quartz; C – corundum; B – beta-aluminium oxide; A – aluminium (marked with vertical red lines; R – calcium aluminates; F – faujasite; L – calcite).

In Figure 6, the XRD patterns obtained for PG30, FCCPGm and BFSPGm can be observed. The X-ray diffractogram corresponding to the ground PG sample (PG30) shows peaks from metallic aluminium (A, JCPDF card #040787) and aluminium oxide in the crystallized phases of corundum (Al_2O_3, JCPDF card #100173) as well as of beta–aluminium oxide (β-Al_2O_3, JCPDF card #100414). Traces of quartz (SiO_2, JCPDF card #331161) and calcium aluminate (Ca_3AlO_6, JCPDF card #320150) were also found.

The patterns for the materials obtained by the co-milling treatment of the precursors with PG presented the following features:

i. The FCCPGm diffractogram showed the peaks in agreement with a zeolite named faujasite ($Na_2Al_2Si_4O_{12}{\cdot}8(H_2O)$, JCPDF card #391380), which correspond with the intense peaks in the FCC diffractogram [14]. Furthermore, the peaks of aluminium (A, JCPDF card #040787), corundum (Al_2O_3, JCPDFcard #100173) and traces of calcium aluminate (Ca_3AlO_6, JCPDF card #320150) and quartz (SiO_2, JCPDF card #331161) indicate the presence of PG addition. A baseline deviation in the 15º-30º range was observed, which was related to the presence of an amorphous fraction (rich in silica and alumina) in the FCC.

ii. In the XRD pattern for BFSPGm, an important baseline deviation between 25º and 35º can be observed because of the typical amorphous phases (Ca-Si-Al oxides) in the BFS mineralogical composition [24]. Overlapping of peaks attributable to the presence of crystalline products due to the presence of PG can be seen: calcite ($CaCO_3$, JCPDF card #050586), BFS and aluminium (A, JCPDF card #040787), corundum (Al_2O_3, JCPDF card #100173) and traces of calcium aluminate (Ca_3AlO_6, JCPDF card #320150) and quartz (SiO_2, JCPDF card #331161).

The peaks above 2Θ =35º corresponding to aluminium are highlighted in red (Figure 6) for 2Θ values of 38.45º, 44.71º and 65.09º (corresponding to the [111], [200] and [220] Miller planes). It is evident the presence of metallic aluminium in PG30, FCCPGm and BFSPGm samples due to the co-milling treatment of the precursors with PG. These results suggested that the aeration reaction of FCCPGm and BFSPGm might be possible due to the metallic aluminium dispersed in the co-milled precursor.

The FESEM micrographs and EDX analysis of selected analysis spots from the PG, PG30, FCCPGm and BFSPGm particles are shown in Figure 7.

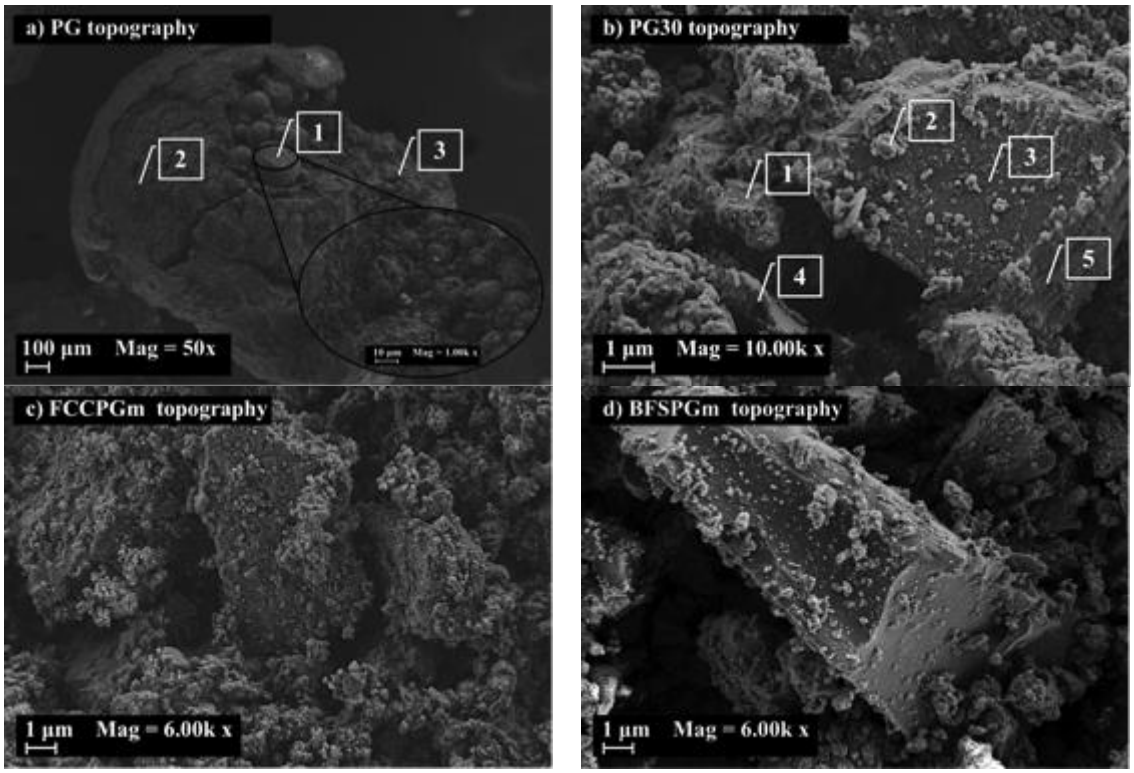

Figure 7 FESEM micrographs: a) PG, b) PG30, c) FCCPGm and d) BFSPGm. Some spots are marked in the micrographs where EDS analysis was done.

The PG was found to have large spherical and spheroidal particles, which had a high porosity (Figure 7(a)). In the case of PG30 (Figure 7(b)), the particle fineness increased because the original spherical and spheroidal particles were completely broken. The presence of aluminium (element) was indicated by the analysis and high aluminium contents were found in PG and PG30 powders (spot 1 in Figure 7(a) with 82.9% and spot 1 in Figure 7(b) with 70%). Considering the oxygen content from these EDS data, part of this aluminium element is chemically combined to Al_2O_3 formation. The resultant metallic aluminium in the EDS analysis was between 22%-64% for the PG sample (spots 1–3 in Figure 7(a)), and 23%–70% for the PG30 sample (spots 1-5 in Figure 7(b)).

In case of the FCCPGm and BFSPGm particles, no evidence of the PG co-milled presence was found in the FESEM micrographs or in the spectra obtained by the EDS analysis. Figures 7(c) and 7(d) show the typical texture for the ground FCC and BFS samples, respectively. The FCCPGm (Figure 7(c)) is characterized by the presence of particles about 20 μm in diameter with particles adhering to their surfaces that are less than 2 μm in diameter. The chemical analysis showed their composition to consist of large amounts of silicon and aluminium, where Si = 21.78 %, Al =28.97 and O = 49.33 %. In the case of BFSPGm (Figure 7(d)), the larger particles were observed to be about 30 μm in diameter with a surface covered in smaller particles (with a lower content than the FCCPGm sample). From the EDX analyses, a high content of calcium and some amount of silicon, magnesium and aluminium were detected (Ca = 31.13 %, Si = 13.7 %, Al = 7.26 %, Mg = 4.78 % and O = 43.12 %).

3.2 Application in alternative cellular concretes manufacture

The density and compressive strength obtained for the GCCs and AACCs (prepared with several PG addition modalities) are shown in Figure 8. The following dosages were selected: a) for PG, an addition of 5% and 10% by weight of the precursor; b) for PG30, 1%, 1.5% and 2%; and c) for the co-milling of PG it was 2% by weight and precursor (BFS or FCC). They were compared to GCCs and AACCs with 0.2% commercial powdered aluminium (A) (see Table 2).

In general, the BFS samples yield higher densities and better mechanical behaviour respect FCC samples independent of the PG addition modality. These results are in contrast with those reported by Font et al. [15]. In that study, when recycled aluminium foil was used as the aerating agent, the FCC-based GCCs yielded higher densities and better mechanical behaviour with respect those obtained for BFS-based AACCs. This can be attributed to the differences in the mixed sample volumes and in the w/b ratio. Yang et al. [32] established that the dry density of alkali activated slag cellular concretes depends on the unit binder content, regardless of the type of precursor used.

There were changes in the density evolution when different PG addition modality was carried out that is rather similar for the use of both precursors, FCC and BFS. When PG was used as the aerating agent, higher densities were obtained for 10% PG with respect to the 5% samples. Specifically, the difference was 15% higher for FCC10PG vs. FCC5PG (Figure 8(a)) and 9% higher for BFS10PG vs. BFS5PG (Figure 8(b)). These results are in contrast with the those observed from the H_2 emission test results. In FCC10PG and BFS10PG, a vigorous chemical reaction was observed due to the large amount of H_2 released. The paste consistency was fluid and it did not have enough resistance (viscosity) to maintain the gas bubbles into the matrix before hardening. Despite the fact that there was a large amount of bubbles, the H_2 was released from the material and the aeration was not effective. For this reason, it was not possible to test a higher percentage of PG addition. When the percentage of PG was decreased by half (FCC5PG and BFS5PG), a more progressive reaction was noted and there was not a large amount of gas released from the matrix. The FCC5PG samples yielded densities that were 24% higher than the control samples (FCC0.2A). The BFS5PG density was 40% higher than the corresponding control material (BFS0.2A). This can be explained by considering the above discussion about the H_2 emission tests. The corresponding amount of PG addition modality to release the corresponding gas that is released by 0.2 % of A addition was 12%-13 % (by wt% precursor). However, the strong chemical reaction in the alkaline medium of the mixes made this percentage addition impossible. Furthermore, it can be considered that the PG particle size was too high and consequently, the gas generation was not homogeneously dispersed into the matrix. Thus, large bubbles were formed and they had a substantial pressure and escaped from the mixture.

With the use of PG30 as the aerating agent, the densities were higher than, or similar to, those obtained with the PG. Compared with FCC5PG, the density of the FCC1PG30 increased 30% and for FCC1.5PG30, it was close to FCC5PG and decreased 4% (Figure 8(a)). In the BFS samples (Figure 8(b)), compared with BFS5PG, the densities increased 44% and 16% for BFS1PG30 and BFS1.5PG30 samples, respectively. The chemical reaction from the 1% and 1.5% addition percentages of PG30 was apparently slow and controlled. However, not enough H_2 was released with the addition of 1% of PG30. The FCC1PG30 density was close to 1000 kg/m^3 and the BFS1PG30 density was higher than 1000 kg/m^3. When 2% of the PG30 was added, a natural density reduction was observed for the FCC samples (5% respect FCC5PG). Nevertheless, there is a slight increase in BFS2PG30 density compared to the BFS5PG (6%). As demonstrated from the H_2 emission test results, a lower quantity of milled material (PG30) with respect the original PG is required to produce the aeration level equivalent to 0.2 % of the metallic aluminium powder in the GCCs and AACCs.

The milling treatment of PG led to an evident improvement in this reaction. These results can be explained by the increase in the specific surface area of the metallic aluminium, which involves a higher contact and reactivity in alkaline medium.

The lowest densities were obtained when the addition was carried out by the co-milling treatment (FCCPGm and BFSPGm samples). It is highlighted that the PG percentage addition was 2%, the same as for the FCC2PG30 and BFS2PG30 samples. The density values for the FCC2PGm and BFS2PGm samples were close to the control samples and yielded 4% and 7% higher densities, respectively. It is remarkable that the PG co-milling with the precursor was an excellent treatment compared to the individual grinding in terms of the obtained cellular concrete density. In the co-milling process, the effectiveness of the particle size was higher and the dispersion of the ground PG particles was better than that obtained by mixing the ground precursor and the ground PG.

From the mechanical point of view, two aspects can be discussed: i) there was an evolution with the curing time in all of the tests, which was attributed to the progress of the reaction with curing time at room temperature; and ii) the improvement of density (lower values) corresponded to a compressive strength reduction (lower values) independent of the PG addition modality. This link between the density and compressive strength is typical for cellular concretes (traditional systems as well as geopolymeric or alkali-activated systems), and it has been reported by several authors [3,5,7,32,33]. There is an exception in this behaviour in the case of FCC2PGm, which had a low natural density (612 kg/m^3) with a high compressive strength (6.2 MPa) compared to the other PG modalities (Figure 8(a)).

In general, the PG co-milling process with the precursors (FCC and BFS) became a practical and effective method for alternative cellular concrete production. The FCC2PGm had a compressive strength of 6.2 MPa after 28 days with a density of 612 kg/m^3. These parameters being similar to those presented for the control sample (FCC0.2A) that had a compressive strength of 5.4 MPa and density of 590 kg/m^3. In a parallel way, for BFS, the sample containing the co-milled PG (BFS2PGm) had a compressive strength of 6.4 MPa and density of 695 kg/m^3. The control (BFS0.2A) had a compressive strength of 7.8 MPa and density of 651 kg/m^3. The 2% addition of this by-product produced GCCs and AACCs with the physical and mechanical characteristics similar than those obtained when 0.2 % of the commercial aluminium powder is added. This discussion is in accordance with that affirmed by Font et al. [14,15], where the most effective method was to incorporate the recycled aluminium foil into the mixes by co-milling with the precursor.

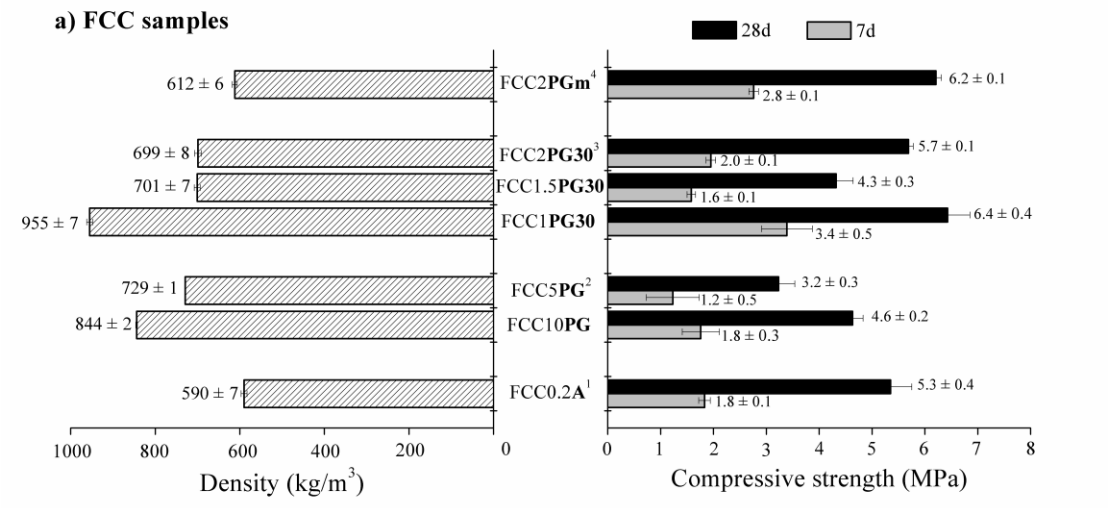

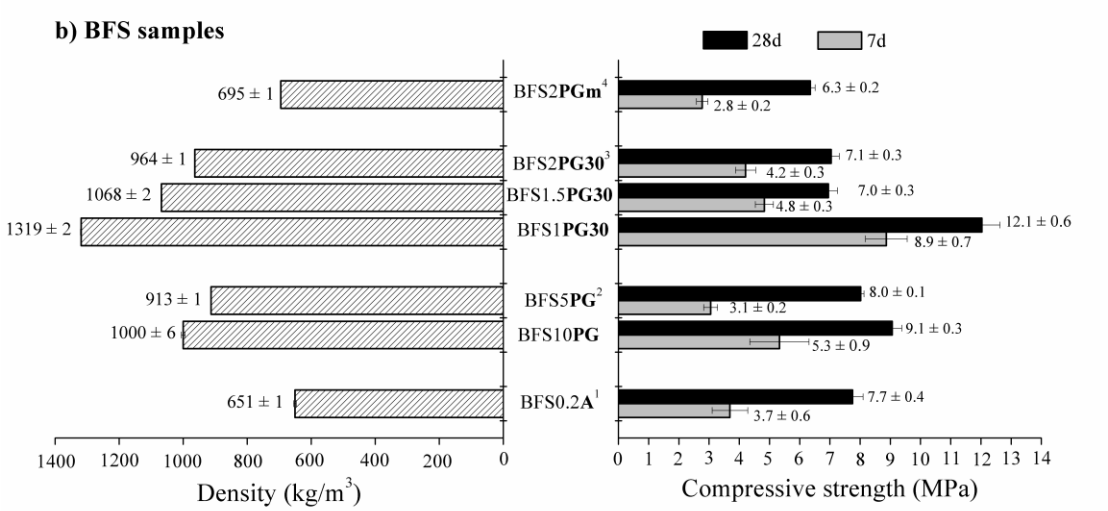

Figure 8 Natural densities and compressive strengths after 7 and 28 curing days for alternative cellular concretes that compares the aeration effect of PG modality: a) using FCC as precursor (GCC) and b) using BFS as precursor (AACC).
1 commercial aluminium; **2** PG; **3** PG 30 minutes milled; **4** PG co-milled with the precursor.

A stable void system with a homogeneous pore size and distribution is the key to providing a stable cellular concrete matrix that has good mechanical behaviour and low thermal conductivity [32,34]. Narayanan and Ramamurthy [35] reported that in cellular concretes, the zone between the cement paste and the voids represent a transition zone equivalent to the interface of cement paste with aggregates from traditional concretes. The density and the mechanical behaviour are related to the thickness and the compactness of this transition zone. The development of the regular void system (shape and size distribution) directly influences in the density and compressive strength of the cellular concrete [34,36].

The void system configuration was analysed and compared for the PG, PG30 and PGm samples (10% wt% for PG and in 2% for PG30 and PGm). Figures 9 and 10 show the FESEM micrographs, OM photographs and the void measurements tables for the FCC and the BFS studied samples, respectively. Upon comparing the influence of the PG modality incorporation in the samples, the size of the pores is generally smaller when the PG particle size is lower. When PG10 is added to the matrix, the aeration was faster and aggressive and involved the development of large pores with irregular shapes, which are interconnected (Figures 9(a1), 9(b1), 10(a1) and 10(b1)). The fresh paste is not consistent enough to entrap the generated hydrogen and the bubbles coalesce and escape. This situation is attenuated by the milling treatment of PG (when PG30 is used), as can be observed by the FESEM data (Figures 9(a2) and 10(a2)). These samples presented a homogeneous distribution of voids with more regular shapes. The number of voids increased with the use of the finer PG powder, and was sometime located in the intermediate zone among the bigger pores. The best results were produced by FCCPGm (Figure 9(a3) and 9(b3)) and BFSPGm (Figures 10(a3) and 10(b3)), in which the reaction developed more slowly and the matrix retained the gas. In these samples, the void system appeared to be in a stable configuration and had a homogeneous range of sizes.

In general, two different imperfections in the void system configuration can be seen: Despite findings by Narayanan and Ramamurthy [35] about the stronger transition zone in cellular concretes than in traditional concretes, some voids have an irregular shape due to the fracture of its transition zone.; Also, there are some unions between voids that are caused by the fracture of the wall among them. These two irregularities are a consequence of the strong gas pressure from the aerating reaction in the fresh matrix. During hardening, the paste does not have enough resistance to entrap the gas without breaking.

J. Alexanderson [36] established a void system classification with differences between macropores (from the mass expansion caused by aeration) and micropores (distributed in the paste among the macropores). The small voids with a mean diameter lower than 100 μm were referred to as micropores and the bigger voids that have mean diameter equal or higher than 100 μm were referred to as macropores. The micropore and macropore size range intervals were assessed as a difference between the smallest and the biggest one.

Analysing this distribution with the obtained results of density and compressive strength tests, the following observations can be made:

- For the FCC samples, the highest density and lowest compressive strength occurred for sample FCC10PG. This material yielded a micropore size range lower than for FCC2PG30 and a macropore size range larger than FCC2PG30 (Figures 9(a1) and 9(b1) compared to Figures 9(a2) and 9(b2)). These ranges mean that for FCC10PG, the micropores had a more regular and constant size distribution and the macropores had more irregular sizes compared to FCC2PG30. Considering the large number of large pores and their irregular shape, when PG was added without a milling treatment (FCC10PG sample), the paste was less consistent because of the interconnection between the voids. By comparing FCC2PG30 with FCC2PGm (Figures 9(a2) and 9(b2) compared to Figures 9(a3) and 9(b3)), both the micropore range and the macropore range were lower when PG was co-milled with the precursor. The FCC2PGm samples had a good pore distribution with homogeneous mean void diameters with respect to the FCC2PG30 pore distribution. Subsequently, the void system structure was more homogeneous without pore interconnections and had a stable paste matrix (Figures 9(a3) and 9(b3)). These observations could explain the discussion above about the lowest density and highest compressive strength for the FCC2PGm.

- In the case of the BFS mixes, BFS10PG had the highest density and mechanical strength. For this sample, the macropore range was similar and the range between micropores was lower when compared to BFS2PG30 (Figures 10(a1) and 10(b1) compared to Figures 10(a2) and 10(b2)). The BFS10PG sample did not present a large amount of micropores and the macropores yielded a more stable and compact paste matrix compared to the other samples. This fact explains its highest density value. For this sample, the aerating reaction was not enough to develop the required cellular structure. Sample BFS2PGm achieved the lowest values of density and compressive strength. In this case, the ranges of both the macropores and micropores were lower than those for the other systems (BFS10PG and BFS2PG30). The BFS2PGm system showed a stable and compact matrix with a homogeneous void shape and without interconnections, which enabled a cellular structure with a low density and sufficient mechanical behaviour (Figures 10(a3) and 10(b3)).

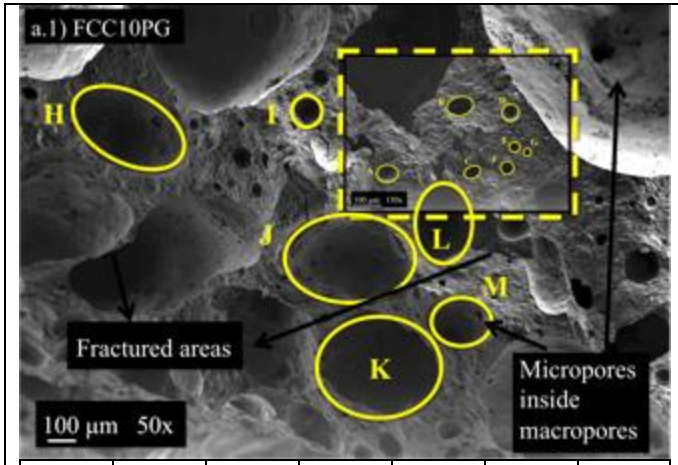

A	B	C	D	E	F	G
66.8	74.1	55.3	52.7	38.0	40.1	30.9
H	**I**	**J**	**K**	**L**	**M**	
488.3	116.1	475.7	446.7	283.2	215.3	

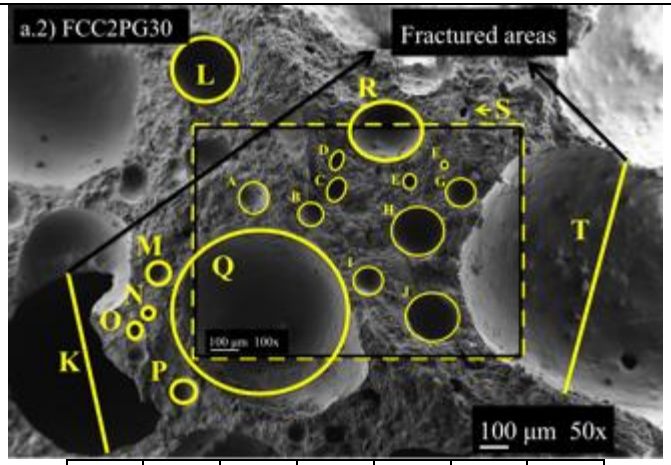

A	B	C	D	E	F	G
106.1	89.3	65.3	57.8	39.7	26.3	105.4
H	**I**	**J**	**K**	**L**	**M**	**N**
192.5	105.1	202.0	752.1	253.3	92.7	45.6
O	**P**	**Q**	**R**	**S**	**T**	
47.6	89.3	719.6	241.2	25.4	832.6	

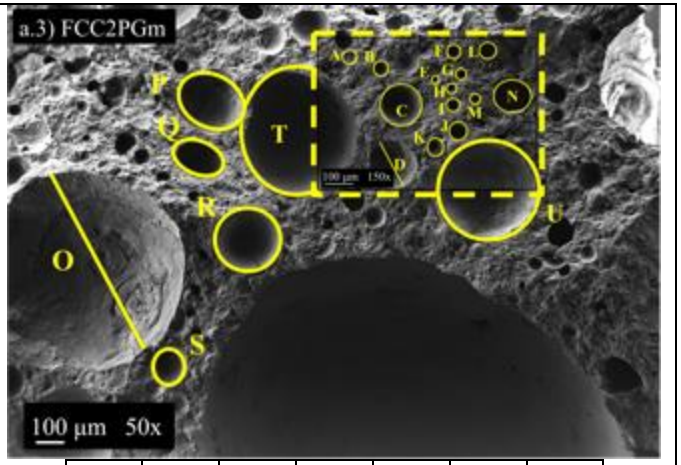

A	B	C	D	E	F	G
52.3	53.6	142.9	169.7	35.1	47.9	39.5
H	**I**	**J**	**K**	**L**	**M**	**N**
48.7	65.4	72.3	70.5	61.0	54.3	130.0
O	**P**	**Q**	**R**	**S**	**T**	**U**
669.9	305.2	253.0	265.5	168.3	384.1	339.4

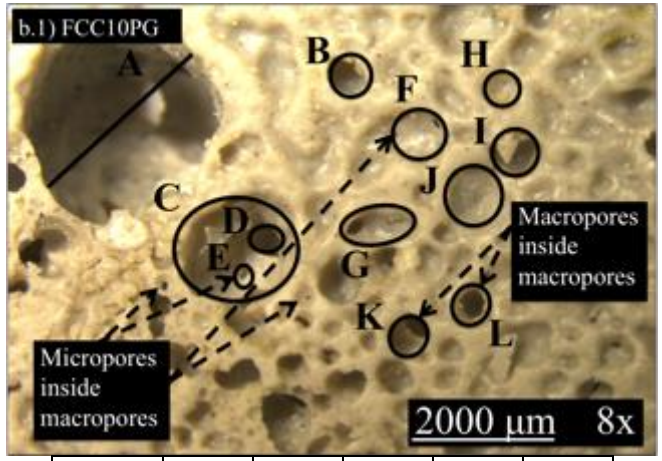

A	B	C	D	E	F
3001	668	1900	551	432	702
G	**H**	**I**	**J**	**K**	**L**
1093	578	665	893	556	592

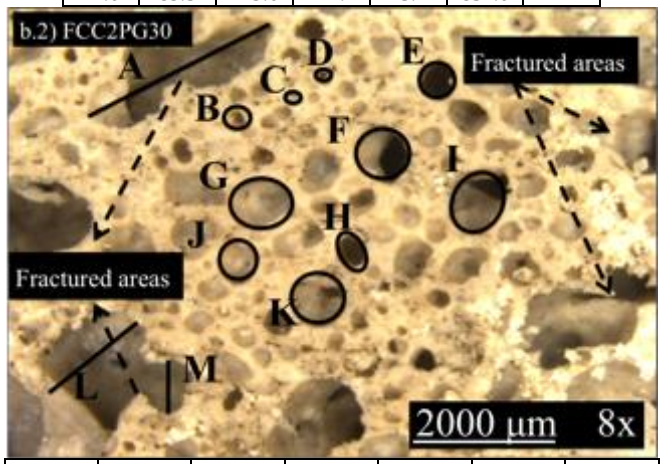

A	B	C	D	E	F	G
2936	376	105	143	675	897	900
H	**I**	**J**	**K**	**L**	**M**	
546	1020	672	724	1520	705	

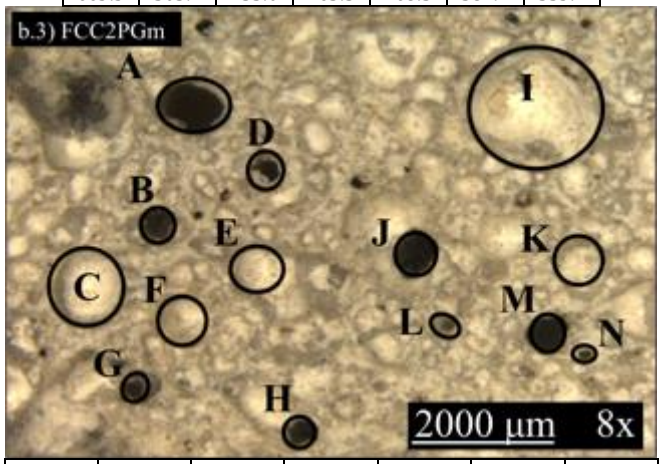

A	B	C	D	E	F	G
944	562	1065	599	765	732	345
H	**I**	**J**	**K**	**L**	**M**	**N**
396	1872	654	709	204	433	198

Figure 9 Void system characterization of GCC based on FCC. Void diameters (with values in µm) measured in: a) FESEM micrographs and b) OM images. For (1) FCC10PG, (2) FCC2PG30 and (3) FCC2PGm samples.

522

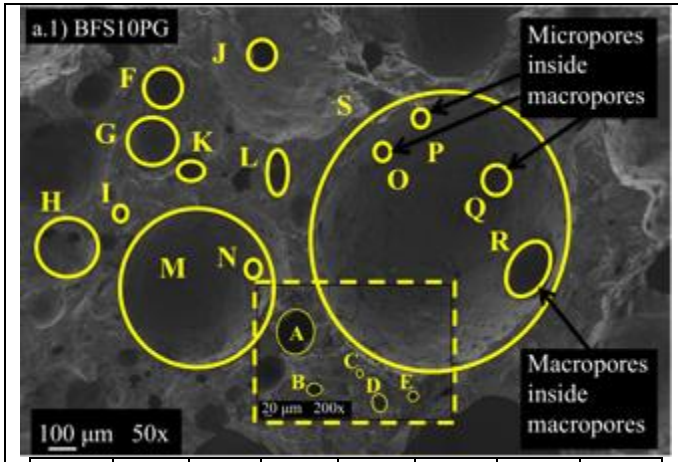

A	B	C	D	E	F	G	H
118.3	44.7	13.4	46.3	29.8	156.3	209.1	322.0
I	**J**	**K**	**L**	**M**	**N**	**O**	**P**
67.3	89.0	70.0	128.8	589.5	72.1	75.6	80.1
Q	**R**	**S**					
102.3	223.0	1090					

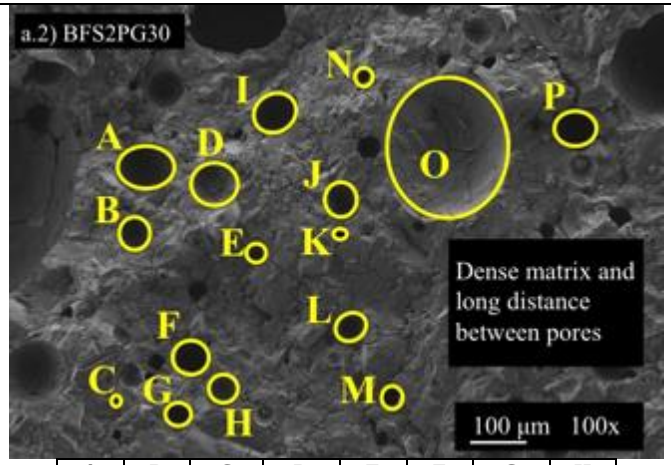

A	B	C	D	E	F	G	H
91.5	52.3	22.2	75.92	35.6	59.5	41.2	47.1
I	**J**	**K**	**L**	**M**	**N**	**O**	**P**
76.5	74.9	28.0	55.4	48.1	36.7	236.7	78.9

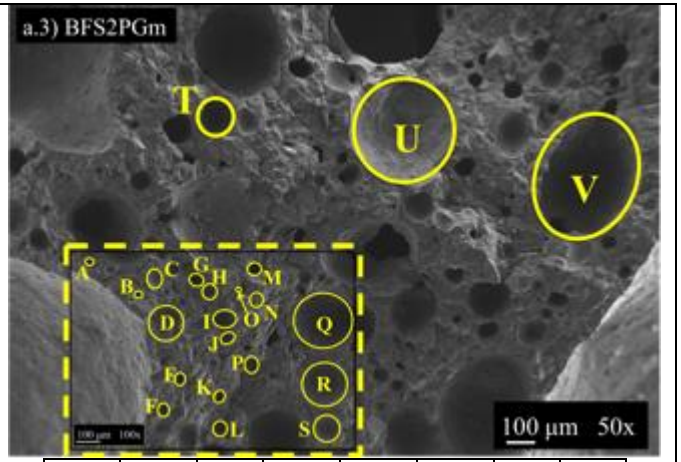

A	B	C	D	E	F	G	H
12.3	13.4	74.1	136.2	44.3	50.9	61.6	70.2
I	**J**	**K**	**L**	**M**	**N**	**O**	**P**
84.8	65.4	38.5	43.7	46.5	51.0	12.1	63.8
Q	**R**	**S**	**T**	**U**	**V**		
218.4	187.6	94.3	192.3	370.7	464.0		

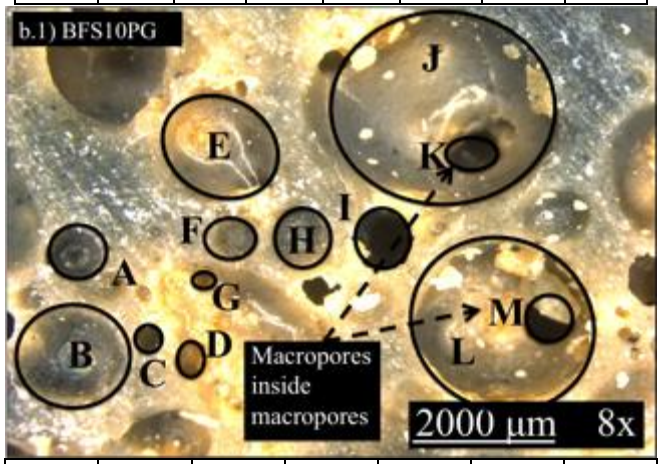

A	B	C	D	E	F	G
674	1982	187	334	1640	676	174
H	**I**	**J**	**K**	**L**	**M**	
548	612	3102	403	2503	425	

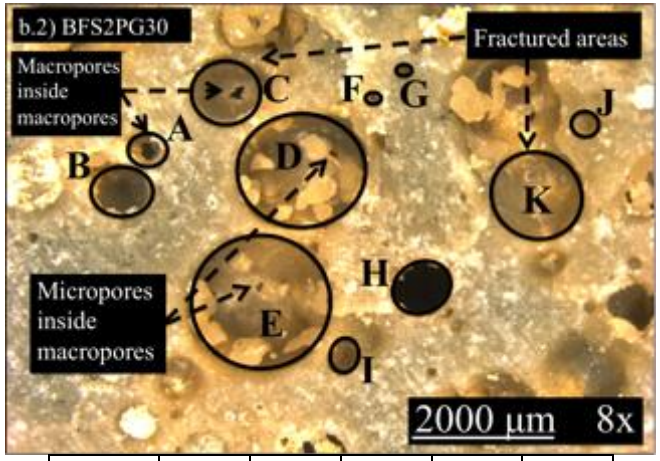

A	B	C	D	E	F
458	987	1198	1697	2157	102
G	**H**	**I**	**J**	**K**	
98.9	549	378	422	1345	

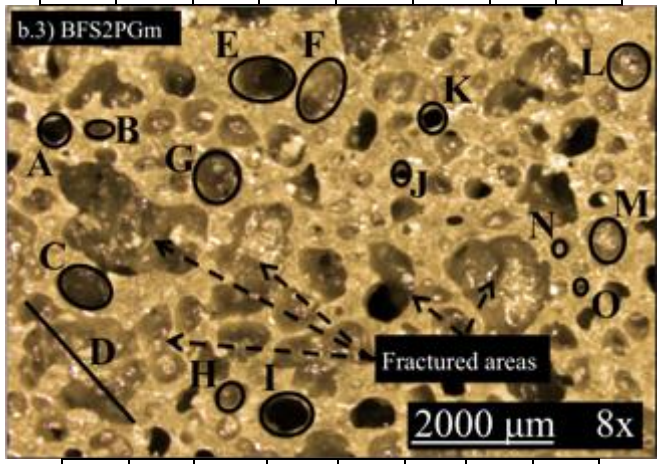

A	B	C	D	E	F	G	H
449	345	754	2212	787	906	873	398
I	**J**	**K**	**L**	**M**	**N**	**O**	
829	392	405	769	673	231	129	

Figure 10 Void system characterization of AACC based on BFS: a) FESEM micrographs and b) OM images. For (1) BFS10PG, (2) BFS2PG30 and (3) BFS2PGm samples.

The results for the density, compressive strength (after 7 and 28 curing days) and thermal conductivity for the FCC2PGm, BFS2PGm and their respective control systems that used 0.2 wt% commercial aluminium powder in are summarized in Table 4 for the 1000 cm^3 samples. There are noticeable differences when the properties that were measured on the 1000 cm^3 samples are compared with the same properties obtained for the 64 cm^3 samples (Figure 8). When a bigger volume of material was manufactured, the density of BFS samples was lower than for the FCC samples. By comparing the 1000 cm^3 vs. 64 cm^3 samples, the densities increased 23% for FCC0.2A and FCC2PGm, and these decreased 10% for BFS0.2A and 13% for BFS2PGm. The differences among the cellular samples were attributed to the w/b ratio and to the mixing methodology.

With these results, is possible to confirm the influence of w/b ratio on the physical characteristics of the GCC and AACC. The metallic aluminium reacts with the alkali and liberates bubbles of hydrogen, which expand the matrix before setting. The paste must have a consistency that prevents the gas from escaping and allows a stable and homogeneous void system to form during the hardening process This in agreement with H. Esmaily et al. [13], who concluded than the density and compressive strength can be more intensely affected by the pore structure than for other manufacturing factors.

Table 4 Density, compressive strength (after 7 and 28 days) and thermal conductivity (28 days) measured for 1000 cm^3 samples.

Sample	Density (kg/m^3)	Compressive strength (MPa)		Thermal conductivity (W/mK)
		7d	28d	
FCC0.2A	726 ± 3	3.9 ± 0.4	6.2 ± 0.2	0.26 ± 0.01
FCC2PGm	753 ± 2	4.1 ± 0.1	6.8 ± 0.3	0.31 ± 0.01
BFS0.2A	583 ± 4	3.8 ± 0.6	7.0 ± 0.2	0.13 ± 0.02
BFS2PGm	602 ± 7	4.2 ± 0.1	7.5 ± 0.1	0.16 ± 0.01

The results from the 1000 cm^3 samples showed a good physical performance in the FCC and BFS samples. The co-milling method of the PG by-product addition obtained densities lower than 800 kg/m^3, which were close to the control values for both utilized precursors. The FCC2PGm had a density only 3.7% higher than FCC0.2A and the BFS2PGm had a density 3.3% higher than BFS0.2A. The compressive strength values increased according to the densities. In comparison to the control samples, the strength for FCC2PGm increased 0.2 and 0.4 MPa after 7 and 28 days respectively. This represents about a 40% compressive strength gain with the curing in this period. In the case of the BFS samples, the compressive strength for BFS2PGm compared to BFS0.2A was 0.4 and 0.5 MPa higher after 7 and 28 days, respectively. This represents about a 45% compressive strength gain with the curing time at room temperature.

With respect to the thermal conductivity, the achieved values were higher with the increased density. For FCC2PGm, the thermal conductivity was 16% higher than the control samples. The same behaviour occurred for the BFS samples. Those yielded a thermal conductivity 18% higher when the PG was used as the aerating agent with respect to the samples that used commercial aluminium powder (BFS0.2A). In any case, the thermal insulating properties for the new alternative environmentally friendly cellular concretes that contained PG were very appropriate.

4. Conclusions

In this work, the effective application of a salt slag recycled by-product (granulated paval, PG) as aerating reagent in alternative environmentally friendly cellular concretes was demonstrated. The following conclusions were drawn from the discussion of the experimental data:

- Chemical analysis indicated that the metallic aluminium content in the PG is the essential requirement for the GCC as well as AACC aeration process. The XRD patterns indicated the metallic aluminium presence in the resultant material when the precursor was milled with PG (FCCPGm and BFSPGm).

- Incorporation of PG into the milling treatment, together the precursor (FCC or BFS), is an excellent method to re-use this by-product in GCC and AACC production. This methodology might improve the productivity and reduce the costs (energy and economic). The fineness of the PG particles and their homogeneous distribution within the particles of the precursor determined the degree of aeration that yielded the most continuous and stable void system distribution in the matrix. The 2% addition of this by-product produced GCC and AACC with the physical and mechanical characteristics close to those obtained when the 0.2 wt% of commercial aluminium was added.

- There were noticeable differences in the physical and mechanical properties for the 1000 cm^3 samples with respect to those obtained for the 64 cm^3 samples. The influence of the void system configuration on the GCC and AACC properties was demonstrated. It was demonstrated that the selection of a suitable w/b ratio could be the key to obtaining a material with the consistency to prevent the gas escaping during the hardening.

- With the commercial aluminium powder replacement by PG in the new alternative environmentally friendly cellular concrete, it is possible to obtain an effective thermal insulating material.

Acknowledgments

The authors give special grateful to Befesa Aluminio S.L (Valladolid, Spain) for the granulated paval supply. The authors would also thanks to Cementval and BPOil for precursors supplying. Thanks are given to the Electron Microscopy Service of the Universitat Politècnica de València (Spain).

Bibliography

[1] C. Meyer, The greening of the concrete industry, Cem. Concr. Compos. 31 (2009) 601–605. doi:10.1016/j.cemconcomp.2008.12.010.

[2] A. Petek Gursel, E. Masanet, A. Horvath, A. Stadel, Life-cycle inventory analysis of concrete production: A critical review, Cem. Concr. Compos. 51 (2014) 38–48. doi:10.1016/j.cemconcomp.2014.03.005.

[3] D.K. Panesar, Cellular concrete properties and the effect of synthetic and protein foaming agents, Constr. Build. Mater. 44 (2013) 575–584. doi:10.1016/j.conbuildmat.2013.03.024.

[4] B. Dolton, C. Hannah, Cellular Concrete : Engineering and Technological Advancement for Construction in Cold Climates, (2006) 1–11.

[5] A.J. Hamad, Materials, Production, Properties and Application of Aerated Lightweight Concrete: Review, Int. J. Mater. Sci. Eng. 2 (2014) 152–157. doi:10.12720/ijmse.2.2.152-157.

[6] A.M. Neville, Properties of Concrete, 2011. doi:10.4135/9781412975704.n88.

[7] N. Narayanan, K. Ramamurthy, Structure and properties of aerated concrete: A review, Cem. Concr. Compos. 22 (2000) 321–329. doi:10.1016/S0958-9465(00)00016-0.

[8] E. Holt, P. Raivio, Use of gasification residues in aerated autoclaved concrete, Cem. Concr. Res. 35 (2005) 796–802. doi:10.1016/j.cemconres.2004.05.005.

[9] K.H. Mo, U.J. Alengaram, M.Z. Jumaat, S.P. Yap, S.C. Lee, Green concrete partially comprised of farming waste residues: A review, J. Clean. Prod. 117 (2016) 122–138. doi:10.1016/j.jclepro.2016.01.022.

[10] T. Luukkonen, Z. Abdollahnejad, J. Yliniemi, P. Kinnunen, M. Illikainen, One-part alkali-activated materials: A review, Cem. Concr. Res. (2018). doi:10.1016/j.cemconres.2017.10.001.

[11] P. Duxson, J.L. Provis, G.C. Lukey, J.S.J. van Deventer, The role of inorganic polymer technology in the development of “green concrete,” Cem. Concr. Res. 37

(2007) 1590–1597. doi:10.1016/j.cemconres.2007.08.018.
[12] V. Ducman, L. Korat, Characterization of geopolymer fly-ash based foams obtained with the addition of Al powder or H2O2as foaming agents, Mater. Charact. 113 (2016) 207–213. doi:10.1016/j.matchar.2016.01.019.
[13] H. Esmaily, H. Nuranian, Non-autoclaved high strength cellular concrete from alkali activated slag, Constr. Build. Mater. 26 (2012) 200–206. doi:10.1016/j.conbuildmat.2011.06.010.
[14] A. Font, M.V. Borrachero, L. Soriano, J. Monzó, J. Payá, Geopolymer eco-cellular concrete (GECC) based on fluid catalytic cracking catalyst residue (FCC) with addition of recycled aluminium foil powder, J. Clean. Prod. 168 (2017) 1120–1131. doi:10.1016/j.jclepro.2017.09.110.
[15] A. Font, M.V. Borrachero, L. Soriano, J. Monzó, A. Mellado, J. Payá, New eco-cellular concretes: Sustainable and energy-efficient materials, Green Chem. (2018). doi:10.1039/c8gc02066c.
[16] R. Arellano Aguilar, O. Burciaga Díaz, J.I. Escalante García, Lightweight concretes of activated metakaolin-fly ash binders, with blast furnace slag aggregates, Constr. Build. Mater. 24 (2010) 1166–1175. doi:10.1016/j.conbuildmat.2009.12.024.
[17] RLG International cementreview, (n.d.).
[18] World Aluminium, Environmental Metrics Report Year 2010 Data Final, (2014) 21.
[19] S.H. Hong, D.W. Lee, B.K. Kim, Manufacturing of aluminum flake powder from foil scrap by dry ball milling process, J. Mater. Process. Technol. 100 (2000) 105–109. doi:10.1016/S0924-0136(99)00469-0.
[20] A. Al Ashraf, Energy Consumption and the CO2 footprint in aluminium production, (2014).
[21] Befesa :: Press :: News archive :: 2013, (n.d.). http://www.befesa.es/web/en/prensa/historico_de_noticias/2013/bma_20130307.html (accessed April 15, 2018).
[22] E.G. de Araújo, J.A.S. Tenório, Cellular Concrete with Addition of Aluminum Recycled Foil Powders, Mater. Sci. Forum. 498–499 (2005) 198–204. doi:10.4028/www.scientific.net/MSF.498-499.198.
[23] Y. Song, B. Li, E.H. Yang, Y. Liu, T. Ding, Feasibility study on utilization of municipal solid waste incineration bottom ash as aerating agent for the production of autoclaved aerated concrete, Cem. Concr. Compos. 56 (2015) 51–58. doi:10.1016/j.cemconcomp.2014.11.006.
[24] J.C.B. Moraes, M.M. Tashima, J.L. Akasaki, J.L.P. Melges, J. Monzó, M. V. Borrachero, L. Soriano, J. Payá, Increasing the sustainability of alkali-activated binders: The use of sugar cane straw ash (SCSA), Constr. Build. Mater. 124 (2016) 148–154. doi:10.1016/j.conbuildmat.2016.07.090.
[25] N.E. En, N. Une-en, española, (2005).
[26] F. Babbitt, R.E. Barnett, M.L. Cornelius, B.T. Dye, D.L. Liotti, S.B. Schmidt, J.E. Tanner, S.C. Valentini, ACI 523.3R-14 Guide for Cellular Concretes above 50 lb/ft3 (800 kg/m3), 2014.
[27] ASTM International, ASTM D5334 - 14 Standard Test Method for Determination of Thermal Conductivity of Soil and Soft Rock by Thermal Needle Probe Procedure, (n.d.).
[28] IEEE 442-1981 - IEEE Guide for Soil Thermal Resistivity Measurements, (n.d.).
[29] D.R. van Boggelen, Safe aluminium dosing in AAC plants, 5th Int. Conf. Autoclaved Aerated Concr. (2011) 45–50.
[30] C.B. Porciúncula, N.R. Marcilio, I.C. Tessaro, M. Gerchmann, Production of hydrogen in the reaction between aluminum and water in the presence of NaOH and KOH, Brazilian J. Chem. Eng. 29 (2012) 337–348. doi:10.1590/S0104-66322012000200014.
[31] Y.A. Aleksandrov, E.I. Tsyganova, A.L. Pisarev, Reaction of Aluminum with Dilute Aqueous NaOH Solutions, Russ. J. Gen. Chem. 73 (2003) 689–694. doi:10.1023/A:1026114331597.

[32] K.H. Yang, K.H. Lee, J.K. Song, M.H. Gong, Properties and sustainability of alkali-activated slag foamed concrete, J. Clean. Prod. 68 (2014) 226–233. doi:10.1016/j.jclepro.2013.12.068.
[33] J.G. Sanjayan, A. Nazari, L. Chen, G.H. Nguyen, Physical and mechanical properties of lightweight aerated geopolymer, Constr. Build. Mater. 79 (2015) 236–244. doi:10.1016/j.conbuildmat.2015.01.043.
[34] E.K.K. Nambiar, K. Ramamurthy, Air-void characterisation of foam concrete, Cem. Concr. Res. 37 (2007) 221–230. doi:10.1016/j.cemconres.2006.10.009.
[35] N. Narayanan, K. Ramamurthy, Microstructural investigations on aerated concrete, Cem. Concr. Res. 30 (2000) 457–464. doi:10.1016/S0008-8846(00)00199-X.
[36] J. Alexanderson, Relations between structure and mechanical properties of autoclaved aerated concrete, Cem. Concr. Res. 9 (1979) 507–514. doi:10.1016/0008-8846(79)90049-8.